Volume 1 | Number 1 | Jan 2013 | Pages 1–100

Journal of
Materials Chemistry B

Materials for biology and medicine
www.rsc.org/materialsB

ROYAL SOCIETY
OF CHEMISTRY

This is an *Accepted Manuscript*, which has been through the Royal Society of Chemistry peer review process and has been accepted for publication.

Accepted Manuscripts are published online shortly after acceptance, before technical editing, formatting and proof reading. Using this free service, authors can make their results available to the community, in citable form, before we publish the edited article. We will replace this *Accepted Manuscript* with the edited and formatted *Advance Article* as soon as it is available.

You can find more information about *Accepted Manuscripts* in the **Information for Authors**.

Please note that technical editing may introduce minor changes to the text and/or graphics, which may alter content. The journal's standard **Terms & Conditions** and the **Ethical guidelines** still apply. In no event shall the Royal Society of Chemistry be held responsible for any errors or omissions in this *Accepted Manuscript* or any consequences arising from the use of any information it contains.

ROYAL SOCIETY
OF CHEMISTRY

www.rsc.org/materialsB

Journal of Materials Chemistry B

PAPER

A Self-assembled Lysinated Perylene Diimide Film as Multifunctional Material for Neural Interfacing

Simone Bonetti,*[a] Mario Prosa,[a] Assunta Pistone,[a] Laura Favaretto,[b] Anna Sagnella,[c] Ilja Grisin,[d] Massimo Zambianchi,[b] Saskia Karges,[a] Andrea Lorenzoni,[a] Tamara Posati,[b] Roberto Zamboni,[b] Nadia Camaioni,[b] Francesco Mercuri,[a] Michele Muccini,[a] Manuela Melucci*[b] and Valentina Benfenati*[b]

We report the design, synthesis and structure properties investigation of a new perylene diimide material (PDI-Lys) bearing lysine end substituents. Water processed films of PDI-Lys were prepared and their self-assembly, morphology and electrical properties in both inert and air environment were theoretically and experimentally investigated. With the aim of evaluating the potential of PDI-Lys as biocompatible and functional neural interface for organic bioelectronics applications, its electrochemical impedance as well as the adhesion and viability properties of primary neurons on the PDI-Lys films were studied. By combined theoretical calculations and electrical measurements we show that due to conversion between neutral and zwitterionic anion, the PDI-Lys film conductivity increased significantly on passing from air to inert atmosphere, reaching a maximum value of 6.3 S x m^{-1}. We also show that the PDI-Lys film allows neural cells adhesion and neuron differentiation and decreases up to 5 times the electrode/solution impedance in comparison to a naked gold electrode. The present study introduces an innovative, water processable conductive film usable in organic electronics and as putative neural interface.

Introduction

Due to the successful applications of organic materials in several electronic devices ranging from transistors, light-emitting diodes and solar cells, during the past few years design and synthesis of new organic materials, with structure-property investigations, have been a matter of intense research efforts. The possibility of fabricating large area, mechanically flexible devices through low-cost processes has promoted the engineering of a variety of material structures, both polymeric and molecular ones, as well as the possible device architectures and functionalities.[1,2] On these lines, the use of organic semiconductors and conductors in biosensors is rising interest for advanced bioelectronic applications.[3–7] Due to their redox properties,[8] high chemical stability, thermal durability and photostability[9] perylene based materials are among the most employed systems.[10–13] Perylene-derivatives are excellent n-type organic semiconductors[14] and have been exploited to realize air-stable high-performance OFETs,[15] light-emitting devices[16] and displayed a significant potential for bio-functional neural interfacing.[17] The construction of ordered functional film materials for the above mentioned applications is an important parameter in developing organic electronic devices. In this context, materials with tunable self-assembly in thin films are highly desirable to obtain control and maximize conductive performances of organic molecules.[18,19] Indeed, controllable self-assemblies of organic conjugated molecules have been shown

recently to be exploitable as a versatile platform to tune thin film materials and devices properties.[20]

In this context, perylene diimide (PDI) derivatives bearing hydrophilic or hydrophobic N-substituents (i.e. attached to the PDI's through an imide bond), showing a variety of supramolecular regular nanostructures[21–23] have been recently reported. Amino acid substituents have also been proposed to promote the formation ofhierarchical supramolecular structures with different degrees of ordering through the site-specific hydrogen bonding and secondary structures intrinsically enabled by the amino acid pendants.[24]

In particular, lysine substitution in perylene was shown to promote self-assembly in controllable nanostructures with tunable dimensions. Depending on the nature of substituent, solvent polarity, and sample concentration, nano-spheres, nanowires, nanobelts, and nanosheets, with different degree of molecular ordering[24] and different electrical properties were obtained.[21,25]

Poly-L-Lysine (PLL) coating of organic semiconductors in multilayer devices is the most common approach to allow cell adhesion and viability otherwise prevented by the organic layer hydrophobicity.[5,26–28] Our previous studies demonstrated that lysine end substitution of a model quaterthiophene semiconductor (T4) enable water dissolution[29] and formation of homogeneous films, while maintaining the semiconductor properties typical for unfunctionalized oligothiophenes and displaying ionic charge transport capability. Moreover, we highlighted the possibility to enhance adhesion of primary neurons on T4-Lys films, a property that is crucial for bioelectronic applications.[7]

On this basis, we envisioned lysine substitution of perylenediimide (PDI-Lys) as a possible strategy to achieve a new molecule usable in organic electronic and as neural interface.

To this end, we introduce here PDI-Lys material and investigate the structure-properties of its water processed films. We show that PDI-Lys is easy processable and forms a compact and ordered film

a. Consiglio Nazionale delle Ricerche (CNR) Istituto per lo Studio dei Materiali Nanostrutturati (ISMN), via Gobetti, 101, 40129 Bologna , Italy
b. Consiglio Nazionale delle Ricerche (CNR) Istituto per la Sintesi Organica e la Fotoreattività (ISOF), via Gobetti, 101, 40129 Bologna , Italy
c. Laboratory MIST E-R, Via Gobetti 101, 40129 Bologna , Italy
d. ETC s.r.l. Via Gobetti 101, 40129 Bologna , Italy Bologna, Italy
† Footnotes relating to the title and/or authors should appear here.
Electronic Supplementary Information (ESI) available: See DOI: 10.1039/x0xx00000x

through simple drop casting. The electrical characterization shows for the first time a peculiar conductive behavior of the PDI-Lys film, further studied and investigated through electrical, optical and computational analysis. In particular extensive theoretical calculations shed light on the peculiar atmosphere dependent electrical behavior of PDI-Lys. Finally, the cast film was tested for the possibility of using this material as active layers, suitable for cell growth and bioelectronics purposes. In particular, we studied the cell viability, the film stability and the impedance at the interface between gold electrode functionalized with the PDI-Lys film and solution i.e. under physiological conditions.

Results and Discussion

Synthesis and film forming properties

The synthesis of PDI-Lys (Figure 1a) involved the coupling of perylene-3,4,9,10-tetracarboxylic di-anhydride with α-Boc-protected Lysine **2** according to the procedure depicted in Figure 1a. Deprotection of the amino group of compound **3** under conventional TFA based acidic conditions afforded the target PDI-Lys **4** in 85% yield after a washing/centrifugation based purification procedure. Combined ^{1}H NMR and ESI-MS techniques (Figure S1 and S2) confirm the PDI-Lys structure. The compounds were

completely dissolved in water only with addition of a low amount of TEA (1 µL/ml H_2O for 1 mg of PDI compound). Cast films of PDI-Lys were prepared by drop casting of 1 mg/ml solution on glass substrates covered with PMMA (Figure 1b) and left to dry under laminar flux. After drying, the film showed a macroscopic homogeneity, a strong substrate adhesion and a thickness of about 500 nm. The latter good filming property of PDI-Lys can be ascribed to the presence of lysine[30] within the material. Indeed, lysine, as an amino acid, allows the self-assembly of the molecule during solvent evaporation and promotes an intense aggregation, maintaining the final nanostructure typical of the perylene diimide derivates. Accordingly, AFM images of the PDI-Lys film show (Figure 1c) a known morphological motif of perylene diimide.[17] A characteristic nanoglobular aggregate texture has been identified and maintained at microscopic level. The image shows that the high homogeneity is maintained also at nanoscopic level.

Electrical characterization

The electrical properties of PDI-Lys were investigated using solution cast films on a PMMA substrate and the conductivity was extracted from the I/V measurements performed from 0 to 60 V (see experimental for device preparation; the device scheme is shown in Figure 2a). The conductivity was calculated for the same device in
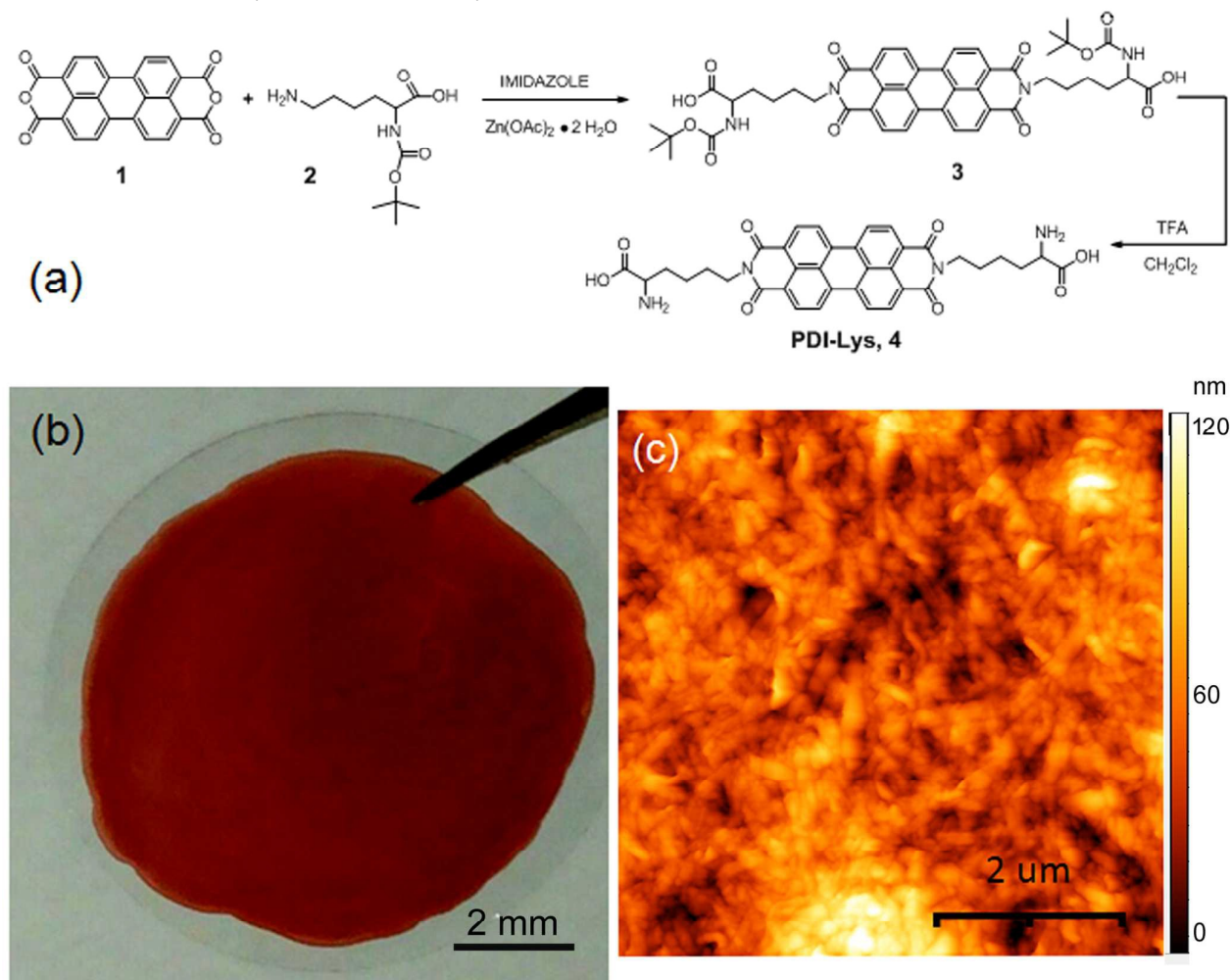

Figure 1. (a) Synthetic route to PDI-Lys, 4. (b) Macroscopic image of PDI-Lys solution 1 mg/ml cast film on glass coverslip PMMA covered and (c) AFM image of the PDI-Lys film.

two different conditions: in air after fabrication and in inert atmosphere (devices kept in an N_2 filled glove box with moisture and oxygen concentration < 0.1 ppm) after 10 days of storage under the same condition. Figure 2a displays the I/V curves obtained in the two conditions. PDI-Lys films in inert atmosphere show a conductivity of 6.2 S m^{-1}, i.e. six orders of magnitude higher than that exhibited by the same sample in air (1.0x10^{-6} S m^{-1}). The same order of magnitude of conductivity was calculated under inert atmosphere for devices prepared with different substrates and electrode materials (Table S1) .The outstanding conductivity of casted PDI-Lys under inert atmosphere is of the same order of magnitude of other lysine functionalized PDI derivates, which are able to show similar values when aggregated as 1D structures,[21,31] nanostructures[24] or when doped with hydrazine.[21,25] The samples left in inert atmosphere for 1 or 10 days showed a different conductivity, lower at short storage and higher after 10 days. To study this phenomenon we moved the samples from air into inert atmosphere and we measured the change of the film resistance while applying a constant bias of 40V. As shown in Figure 2b, the resistance decreases over time with a roughly linear trend. Figure 2b also suggests that the increase of the conductivity could be due to a "purification" effect under N_2 atmosphere and not due to the applied bias. Indeed, when switching off the bias and applying again the bias after different timing, the increase of conductivity is maintained as a linear function of the total time.

For in depth understanding of the effect of air on PDI-Lys

conductivity, the absorption spectrum of casted films was measured in air and inert atmosphere. As shown in Figure 2c, the typical $\pi - \pi^*$ ($S_0 \rightarrow S_1$) transition of perylene diimide core around 478 nm is clearly visible in air as well as in inert atmosphere. In addition, two absorption peaks related to dimer excitation are shown at about 500 and 550 nm. It is noteworthy that the dimer excitation peaks of PDI-Lys in air are slightly red shifted if compared to those in inert atmosphere (Table 2). Moreover, two more peaks at 732 and 818 nm characterize PDI-Lys in inert atmosphere. Therefore it can be concluded that the environment determines different molecular interactions in the solid state. To confirm these results, the absorption spectrum of PDI-Lys films kept in air for just 1 minute was measured. As shown in Figure 2c, the 732 nm and 818 nm peaks rapidly decrease as well as the dimer excitation peaks are slightly red shifted, thus proving that the spectral properties of the film approaches those of PDI-Lys stored in air for a long time. To understand if this behavior was comparable with the electrical properties we observed in air, a device stored in inert atmosphere for 1 day was measured immediately after air exposure. A low constant bias was imposed (5V) to avoid a possible degradation in air. As shown in Figure 2d, we observed a steep drop of the conductivity of the PDI-Lys film in the first minutes followed by a slow decrease during the remaining time. Hence, the described electrical behavior is directly correlated with the drop of the two peaks at 732 and 818 nm observed in the spectra of PDI-Lys films under inert atmosphere (Figure 2c), mainly resulting from air
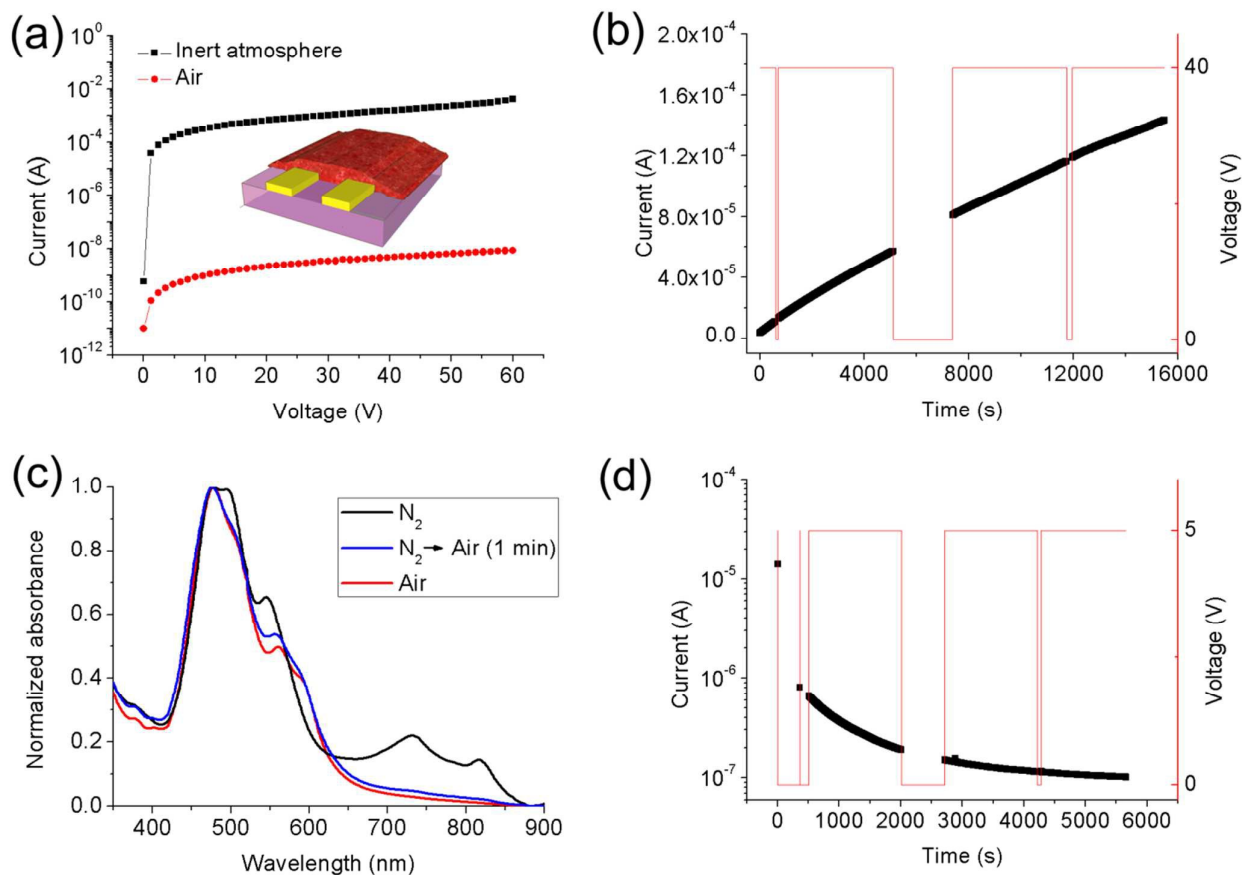

Figure 2. (a) I/V in air and N_2 inert atmosphere of casted PDI-Lys film. (b) Measurement with a 40 V constant voltage applied in N_2 inert atmosphere PDI-Lys casted film after air conservation. (c) Absorbance spectra of PDI-Lys casted film in N_2 inert atmosphere and in air at different time points. (d) Measurement with 5V constant voltage in air of PDI-Lys casted film after N_2 inert atmosphere conservation.

doping.

Theoretical calculations.

To shed light on the working principle behind the electrical and optical behavior of the PDI-Lys thin film, theoretical investigations were performed.

Initially, MD simulations were carried out to assess the aggregation properties of PDI-Lys molecules in thin films. To this end, a PDI-Lys dimer was first equilibrated in vacuum at temperatures close to those used in the annealing of thin films based on perylenes (400 K). Upon equilibration, the perylene diimide cores of the dimer are slightly staggered, in agreement with other studies on PDI derivatives.[32] This core orientation can be related to the particular intermolecular interactions between the lysine residues of adjacent molecules. The structure of the equilibrated dimer was then used to model a bi-dimensional crystal of PDI-Lys, which was inserted into an orthorhombic simulation 2D periodic supercell with vacuum along z-axis, annealed at 400 K and equilibrated at 300K. The 2D configuration obtained by MD simulations was subsequently used in DFT calculations, performed on a representative dimer extracted from the relaxed crystal structure. DFT/B3LYP calculations indicate that the HOMO and LUMO orbitals of PDI-Lys in the neutral state (Figure S3) are strongly localized on the aromatic core, as expected for alkyl-functionalized PDIs. Indeed, the computed electronic energy of frontier orbitals of PDI-Lys (HOMO -5.97 eV, LUMO -3.43 eV) is very close to that of a methyl-substituted PDI (HOMO -5.96 eV, LUMO -3.42 eV). Consequently, all subsequent DFT calculations on PDI-Lys were performed on simplified models in which the lysine moieties are replaced by a methyl group.

In wet conditions or aqueous solution with physiological pH, however, the lysine substituents of PDI-Lys are expected to exist in their more stable zwitterionic form (see Figure 3), involving a proton transfer from the carboxyl acid to the amino group.
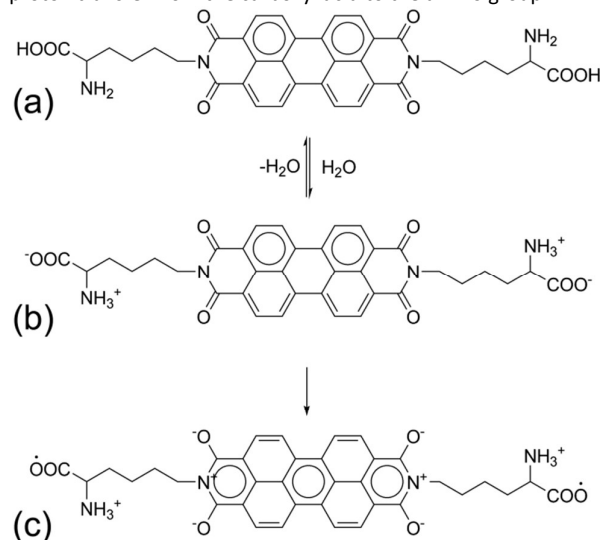
Figure 3. (a) Structure of PDI-Lys in the neutral and (b) zwitterionic forms and (c) double-radical resonance hybrid.

The subsequent evaporation of water related to the formation of a thin-film by drop casting, and the consequent lack of solvation can potentially induce a rearrangement of the charge distribution. Namely, a possible charge reorganization induced by dehydration may involve the formation of carboxylate radicals and ionization of the imide groups, as shown in Figure 3.

Notably, the stability of the molecule shows in Figure 3b is supported by the enhanced aromaticity, as predicted by Clar's sextet theory.[33] In addition, the electronic structure of same molecule can be described in terms of a manifold of resonance isomers, with a different charge distribution, including partially ionized forms and structures with a negative charge strongly localized on the π core of the molecule (see Figure 4).

The localization of charge in the radical zwitterion form, as evidenced by the resonance hybrid as shown in Figure 4c, leads to an increase of free charge carriers in PDI-Lys aggregates and can be considered as responsible for the observed outstanding conducting properties of PDI-Lys at the solid state. This finding is consistent with previous experiments on the formation of anions in thin-films of PDI derivatives, realized by introducing nucleophilic N-groups in the bay substituents of the perylene core.[34,35]
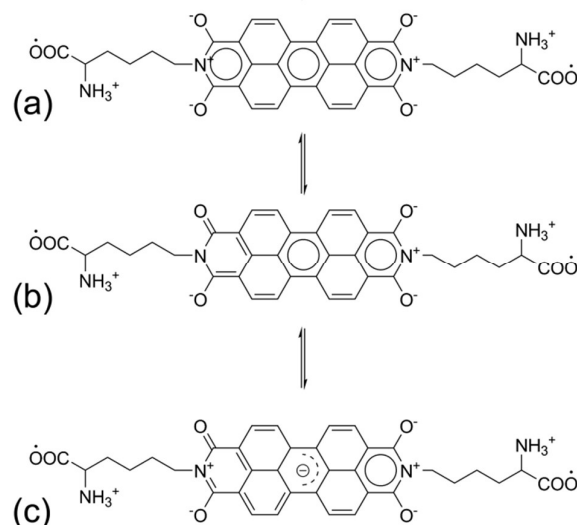
Figure 4. Resonance hybrids of PDI-Lys in the zwitterionic form with (a) three and (b) two localized aromatic sextets and with (c) electron localization in the perylene core.

The dependence of the protonation state and electronic structure of PDI-Lys on the environment and aggregation was assessed by UV/VIS absorption spectroscopy and comparing measured spectra with TDDFT computed transition energies. The absorption spectrum of PDI-Lys in aqueous solution (Figure S4) reflects the typical behavior of coexisting monomers and dimers of perylene diimides:[36] the π-π* ($S_0 \rightarrow S_1$) excitation involving the perylene core exhibits a main (0-0) transition at 514 nm and two peaks at 477 nm and 457 nm, corresponding to the 0-1 and 0-2 vibronic transitions, respectively (Table2).

The other two strong absorption features, at 555 and 499 nm, respectively, are assigned to dimer transitions involving the two lowest (S_1' and S_1'') singlet states.[37] Accordingly, the relative intensity of the two peaks at 499 and 555 nm, assigned to dimer species, increases with the concentration (Figure S4). Notably, the relative intensity of these two lowest dimer transitions is about 0.5, thus in line with values (≤ 0.7) expected for perylene diimide aggregates.[37] Computed excitation energies for the monomer and dimer species in water are in excellent agreement with the experiment, thus supporting the picture above.

The absorption spectrum of thin-films of PDI-Lys exposed to ambient conditions reflects a molecular environment that can be associated to enhanced aggregation and reduced effects of solvation. Indeed, the measured spectrum can be interpreted as the superposition of the individual spectra of dimer species solvated in

water (508 and 593 nm) and in solvent-free aggregates (475 and 562 nm), as also confirmed by TDDFT calculations.

The situation is dramatically different for thin-films of PDI-Lys after extended exposure to inert atmosphere. Beside typical spectral signatures of unsolvated dimer species (469 nm), as expected for PDI-Lys in inert environment, new significant features appear at higher wavelengths. Namely, the absorption spectrum of PDI-Lys in inert atmosphere exhibits two broad absorption bands, peaked at 732 and 818 nm, not present in air conditions and that can be related to the formation of a perylene anion,[38,39] as also confirmed by TDDFT computed frequencies. The occurrence of absorption peaks in functionalized PDIs in the range between 700 and 850 nm is generally ascribed to radical anions originating by the presence of strong electron acceptor substituents and stabilized by the extended π-conjugation, as also evidenced by cyclovoltammetry measurements.[40] The stabilization of the perylene anion in inert atmosphere agrees with the charge localization of resonance form shows in Figure 4c and accounts for the observed massive enhancement of conductivity with respect to films exposed to ambient conditions.

	Computed	Experimental	Assignment
	-	457 nm	Monomer
	-	477 nm	Monomer
Solution	503 nm	499 nm	Dimer
	518 nm	514 nm	Monomer
	549 nm[a]	555 nm	Dimer
	473 nm	469 nm	Dimer
	498 nm	502 nm	Dimer anion
Thin film in inert environment	543 nm	548 nm	Dimer anion
	575 nm	571 nm	Dimer anion
	690 nm	645 nm	Dimer anion
	725 nm	732 nm	Dimer anion
	830 nm	818 nm	Dimer anion
	-	454 nm	Monomer
	473 nm	475 nm	Dimer vacuum
Thin film in air	503 nm	508 nm	Dimer water
	558 nm	562 nm	Dimer vacuum
	587 nm	593 nm	Dimer water

[a]Value obtained from the TDDFT computed $S_0 \rightarrow S_1$ 0-0 transition (587 nm) and assuming a shift of 0.15 eV for the vibronic coupling[41].

Table 2. Peak position experimental and calculated of 3 different PDI-Lys conditions: solution, thin film in air and thin film in inert atmosphere.

PDI-Lys films as neuronal cells interface.

Our previous studies showed that with respect to the quaterthiophene (T4) and glass coverslips pre-coated with poly-L-Lysine, the adhesion and differentiation of primary neurons were higher in L-Lysine bonded T4 (T4-Lys), highlighting the possibility of using T4-Lys as promising material interface for bioelectronic applications.[7] Moreover, we have also demonstrated that a perylene diimide derivate thin film (P13), fabricated by high vacuum evaporation technique and coated with Poly-D-lysine was suitable to support neuronal adhesion, cell growth, differentiation and preserved excitability properties.[17] Here, to test biological effects of L-lysine linked to perylene diimide, we studied the biocompatibility, interfacing the PDI-Lys film with primary rat Dorsal Root Ganglion (DRG) cell culture, a validated model to determine the regenerative outgrowth capabilities of individual neurons of the Peripheral Nervous System (PNS).[42] To this end, a comparative study was carried out, considering the following conditions: glass coverslips and P13-films coated with poly-L-Lysine (hereinafter listed as glass-PLL and P13-PLL respectively), bare P13 films grown on glass and PDI-Lys films. Cell viability was investigated by fluorescein diacetate (FDA) assay to determine the amount of adherent and living cells. Fluorescent images (Figure 5a), captured after 5 days *in vitro* (DIV), showed viable cells on Glass-PLL, P13-Lys and PDI-Lys, with a morphology resembling the one previously reported for cultured DRG neurons [Benfenati et al., 2012 adv fun mater; Bonetti et al., adv healthcare Mater 2015]. Conversely, only few cells were detected on the bare P13 film.

Cell counting revealed that the highest cell viability was observed in DRGs cells cultured on P13-PLL after 5 DIV (Figure 5b). However, the growth of cells on PDI-Lys was significantly higher compared to bare P13 films (Figure 5b). Indeed, cell adhesion resulted in almost null on bare P13.

In order to verify the impact of PDI-Lys on neurite outgrowth, we stained DRG cell culture with Growth-associated protein (Gap-43). GAP-43 is a major constituent of the axonal growth cone and expressed in cell bodies and outgrowing neurites of fetal and neonatal rat brains and DRG sensory neurons.[43] This protein is used as marker for axonal growth.

Typical micrographs of cells immunostained with GAP43 from P13-PLL and PDI-Lys after 5 DIV are shown in Figure 5c. Gap-43 was highly expressed in cell bodies and neurites (Fig. 5c, white arrows) of both cell culture types, demonstrating the occurrence of axonal outgrowing/regenerating processes in the cells cultured on PDI-Lys films. We also quantified and compared neurite length after 5 DIV (Fig. 5d) in both experimental conditions. The average of neurite length was significantly higher in neurons plated on PDI-Lys compared to those plated on P13-PLL.

Collectively, these results showed that the linkage of lysine improved cell adhesion on PDI-Lys with respect to bare P13 and neurite outgrowth with respect to P13-PLL.

It is remarkable that PDI-Lys enables primary neuronal cell adhesion and growth of neurites extension without the need of any further coating of the interface. In this context, we previously observed that hydrophobicity/hydrophilicity, as well as surface morphology and roughness of the film are considered principal factors mediating cell/substrate interaction [Bonetti et al., 2015]. Contact angle measurements displayed an increased wettability of PDI-Lys in respect to high hydrophobicity of P13 thin films. The data are in agreement with a previous study[17] where we reported on poor wettability of the hydrophobic P13 semiconductor deposited on glass substrate (contact angle value was about 97.9°). On the contrary, the contact angle of the PDI-Lys measured was 43.7°. In this view, the increased wettability of the PDI-Lys compound with
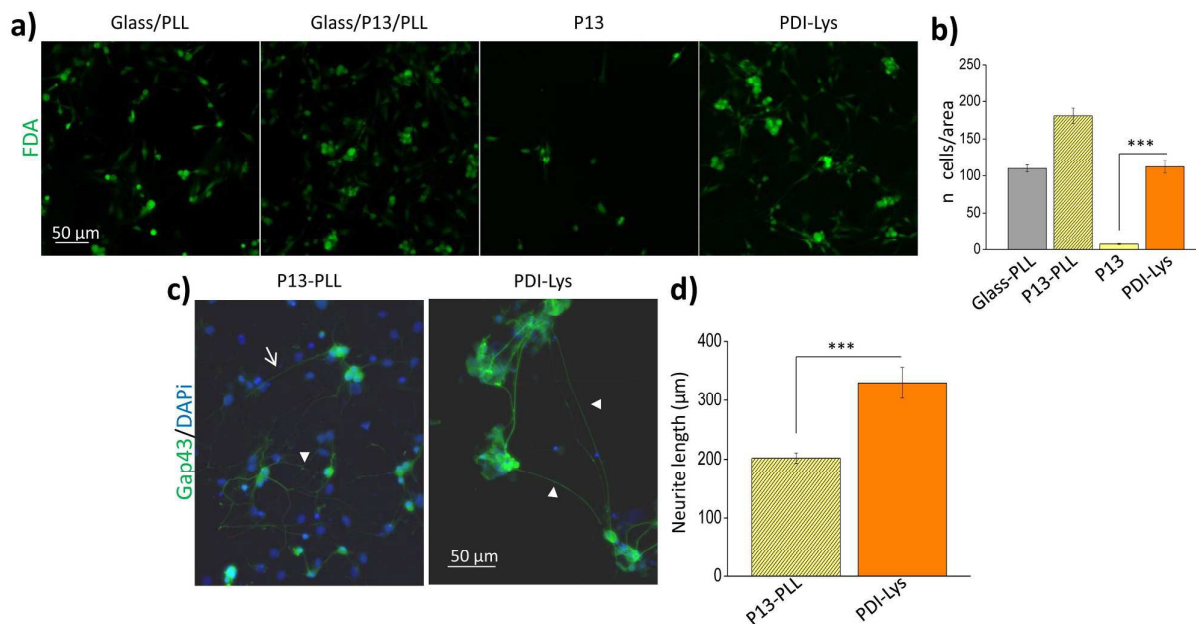
Figure 5. (a) Micrographs representing Fluorescein Diacetate (FDA)-stained DRG culture plated on Glass-PLL, P13-PLL, P13 and PDI-Lys, captured after 5 days *in vitro* (DIV); (b) Histogram plot of the FDA positive cells/areas counted on the same conditions after 5 DIV. A significant difference was observed in cells counted on PDI-Lys compared to P13 after 5 DIV (***p<0.001). (c) Images of DRG culture stained for axonal growth marker Gap43 (green channel). DAPI blue staining marks cellular nuclei. White arrowheads indicate neurites. (d) Histogram plot representing neurite length, measured in neurons grown on P13-PLL (yellow bar) and PDI-Lys (orange bar). n= number of neurites measured for each condition: n=125 for P13-PLL and 81 for PDI-Lys

respect to P13, being a consequence of the functionalization of PDI with L-Lysine, resulted in a greater hydration of the surface and could account for the improved cell adhesion we observed. On the other hand, the overall cell adhesion (neuronal and non neuronal) on PDI-Lys, even though consistent, is significantly lower than the one obtained by coating the glass with PLL. These data are not surprising as they resemble the one obtained for a quaterthiophene lysinated compound named T4-Lys [7]. The homogenous distribution of PLL on glass and the higher availability of lysine moieties for electrostatic interactions with cells on PLL polymer coated glass compared to T4Lys, could possibly account for the increased cell numbers.

According to the fluorescent images reported in Figure 5 and the relative neurite length analyses, it is evident that PDI-Lys supports also DRG neuron differentiation - which is higher compared to P13-PLL. Moreover, the images show the different cell distribution: neurons appeared clustered on PDI-Lys. The soft nature of the organic component of the molecule could account for higher neurite length on PDI-Lys, while the irregular distribution of the Lysine pendant at the interface with the cell or the irregular surface of the material could explain the clustered cell distribution over the PDI-Lys substrate.

Electrochemical measurements.

After the biocompatibility test on neuronal cells to investigate whether PDI-Lys is suitable as a bioelectronic material in electrophysiological application, we checked the application of PDI-Lys film as cover of a gold electrode to improve the bioelectrical signal recording of the naked gold electrode, while maintaining the film stability in physiological conditions. We measured the impedance between 0.5 mg/ml PDI-Lys film casted on top of a gold electrode (PDI-Lys-Au) and 0.1 M phosphate buffered saline (PBS). PBS has the appropriate ionic strength and osmolarity comparable with physiological environment.[44] We used a large area electrode (20 mm^2) to study the integrity of the film and the suitability for the use in *in vitro* and *in vivo* recording. We applied a 10 mV RMS sine wave with frequencies varied logarithmically from 10 Hz to 10 kHz, which is the frequency range of interest for most electrophysiological signals.[45] As a control each PDI-Lys-Au electrode measurement was compared with the closest naked Au electrode. The plots of the impedance magnitude for PDI-Lys-Au and Au electrode are depicted in Figure 6a. For both samples the measured impedance decrease by increasing the frequency of the AC signal. The Au electrode shows a linear impedance increase which is proportional to the decrease of the Log_{10} frequency as well known in literature.[44–46] The impedance values of PDI-Lys-Au are lower compared to the control. Indeed, at 10 KHz the control electrode has an impedance two-fold higher (110 Ω) in comparison to PDI-Lys-Au (50 Ω). At 1 KHz, a frequency of particular importance for the recording of neuronal action potentials, the PDI-Lys-Au electrode has an impedance value five times lower (150 Ω) in comparison to the control gold electrode (810 Ω). The electrode

impedance decreases more than two-fold in comparison to the control also in the lower frequencies near 10 Hz. These results indicate that PDI-Lys material optimizes the coupling between ion and electrical charge carriers, decreasing the impedance value between the electrode and solution. This validates the potential of a simple PDI-Lys casted film covered electrode as a promising tool for neural interfacing and engineering.

To demonstrate the potential of PDI-Lys as interface for this application and the possible limitations due to the film thickness and integrity, we fabricated different PDI-Lys-Au electrodes using four different concentrations of the organic material to obtain a

matching may account for these effects. Films casted with a thickness around 80 nm did not show an impedance value different from the Au control. This phenomenon is explicable observing the Figure 6c and 6d that represent respectively the optical microscope image 50x of the film fabricated using 0.5 mg/ml (Figure 6c) and 0.125 mg/ml (Figure 6d) of PDI-Lys. The films fabricated with 0.5 mg/ml solution are homogeneous and cover the whole electrode surface whereas those fabricated with lower concentrations did not form a proper film but large organic agglomerates on top of the electrode, leaving the gold uncovered by the film. Therefore electrodes exposed to the solution have a major impedance
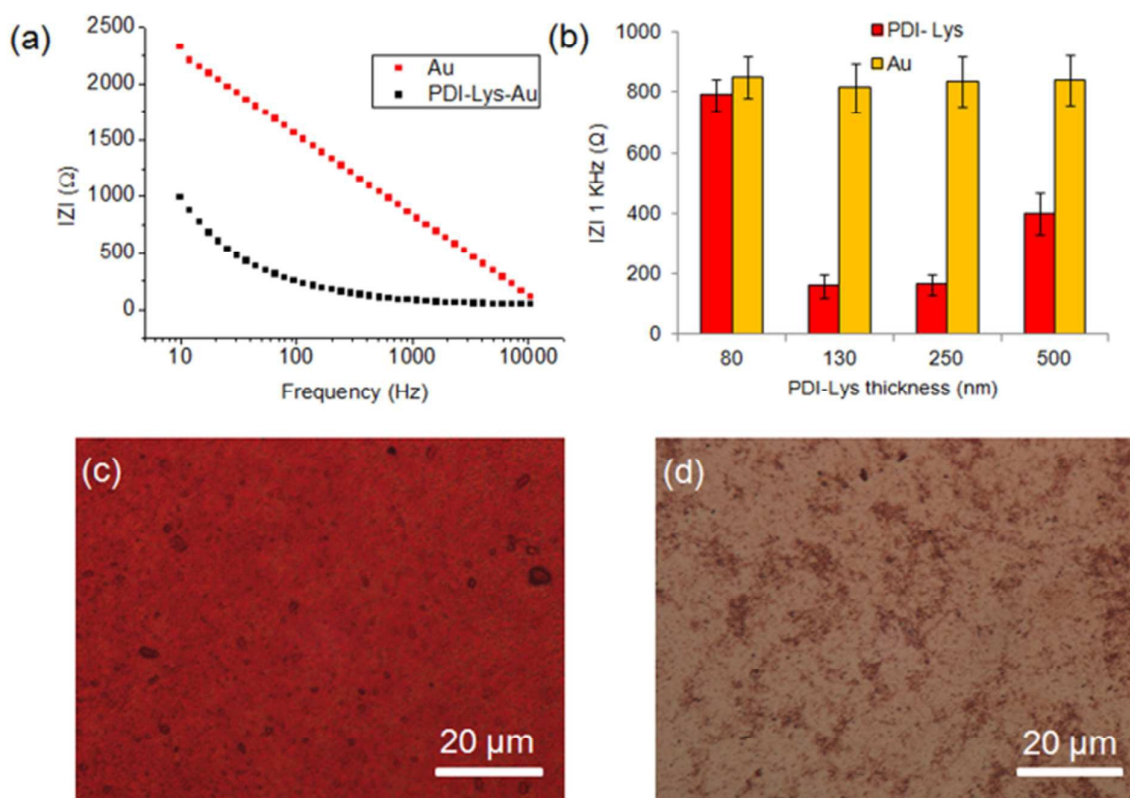

Figure 6. (a) Bode plot of gold electrode and 0.5 mg/ml PDI-Lys electrode in PBS 1x. (b) Difference of 10 Hz impedance between the gold electrode and PDI-Lys electrode using different concentrations of organic molecules (5 samples per condition). (c) Optical microscope images 50X of a PDI-Lys electrode fabricated with 1 mg/ml (c) and (d) 0.125 mg/ml organic molecule solution.

different electrode cover thickness. The histogram plot in Figure 6b represents a statistic study (5 samples for condition) on the impedance magnitude value at 1 KHz.

We fabricated the electrodes using 4 different solution concentrations (1.0, 0.5, 0.25, 0.125 mg/ml) to obtain different coating thicknesses of PDI-Lys films. We obtained a film thickness around 500, 250, 130 and 80 nm, respectively. The film fabricated with the solution concentration of 0.125 mg/ml does not show a high homogeneity after the solvent evaporation, compared to the films obtained with the other thee concentrations.

The impedance of the PDI-Lys-Au electrode is lower than in the Au control when using 500, 250 and 130 nm thick cover films. With 500 nm thick films we obtained a higher impedance value in comparison to 250nm and 130 nm thick film. The increase in the thickness of the covering layer that slightly decreases the electrode-solution

contribution due to the gold exposed in comparison to PDI-Lys aggregates.

To test the long-term stability of the PDI-film we performed 500 cycles of cyclic voltammetry with a potential range of 0-600 mV at a sweep rate of 100 mV s^{-1} in PBS, comparing to the naked gold electrode as control (Figure7a). We imposed a maximum voltage of 600 mV to maintain the solution stable, without inducing water oxidation. The voltammograms show a higher quantity of charge exchange passing from PDI-Lys/solution interface in comparison to the control, demonstrating a better interface with respect to the standard one. However as shown in figure 7b, at the PDI-Lys/solution interface, the maximum value of current (at 600 mV) as a quantity of charge in the full voltammograms (Figure 7c) decreases slowly until it stabilizes at 400 cycles, mimicking the same phenomena as the control (Figure 7d).
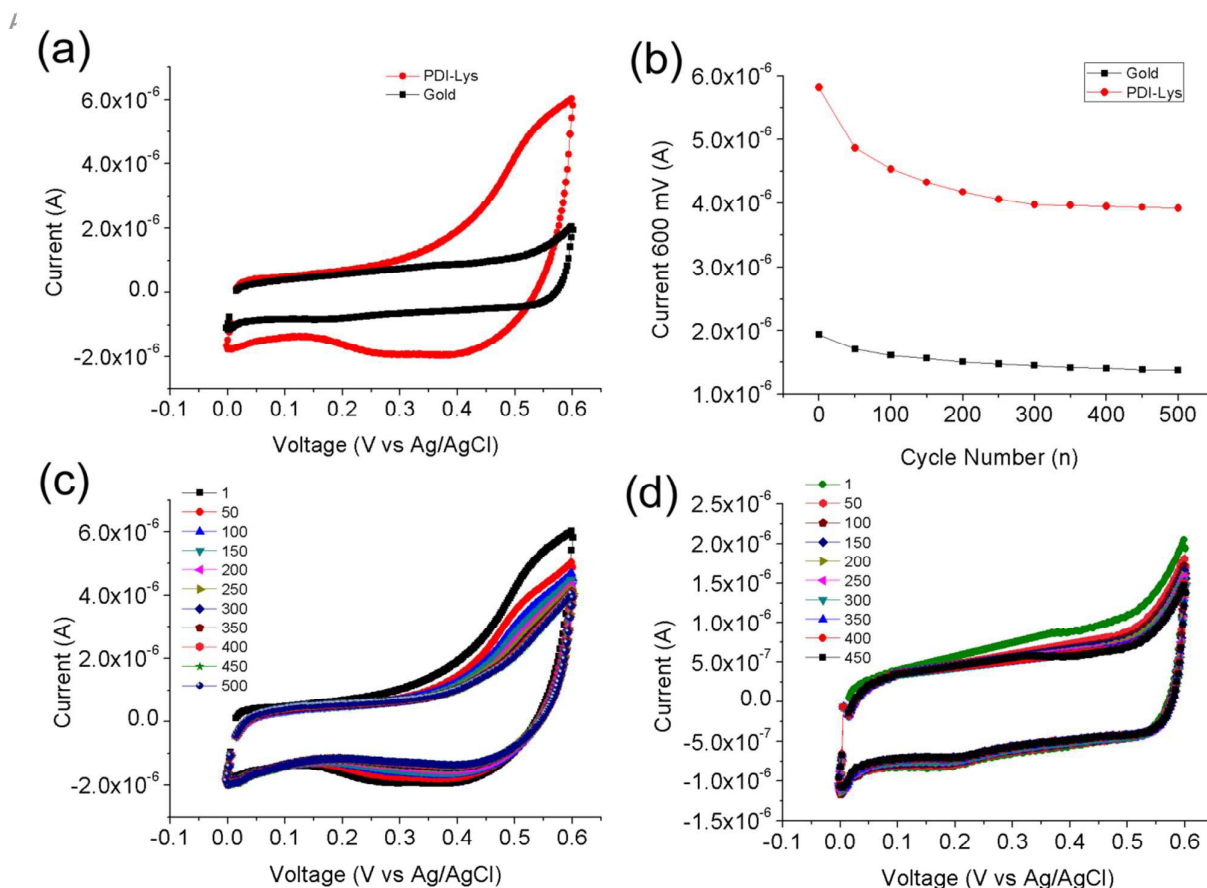
Figure 7. Comparison between PDI-Lys-Au and naked Au electrode voltammograms in PBS 1X (a). Stability test of PDI-Lys-gold and naked gold electrode plotting higher current values each 50 cycles (b). Cyclic scan of PDI-Lys-gold electrode (c). Cyclic scan of gold electrode (d).

The absence of an evident peak in the voltammogram and the slow decreasing after repetitive cycles underline the high stability of the PDI-Lys film in solution within the biological voltage stimulation range.

Collectively, these results indicated the importance of the PDI-Lys film to increase the performance of coupling between electrode and solution maintaining a stability comparable with the control electrode. These results show a promising potential of the PDI-Lys film interface as bioelectronic interface for neural *in vitro* and *in vivo* applications.

Experimental

Chemicals

Perylene-3,4,9,10-tetracarboxylic dianhydride, **1** and L-lysine **2** were purchased from Sigma Aldrich and used without further purification.

Synthesis of PeryleneDiimide Lysine PDI-Lys, 4

Compound **3** was prepared according to a previously reported procedure[8] and purified by repeated washing/centrifugation of the red-violet crude precipitate with CH_2Cl_2, acetone and i-PrOH. Compound **3** was obtained as a dark red powder in 97 % yield. ExSI-MS *m/z* [M-1] = 847,9, ^{1}H NMR (D_2O + TEA) temp=70°C; δ ppm: 7.95 (bm 4H), 7.73 (bm 4H), 4.22 (bs 6H), 1.73 (bm, 30H). Compound **3** (250 mg, 0.3 mmol) was dissolved in 10 ml of a 1:1 solution of TFA and CH_2Cl_2 and stirred at RT for 18 h. The solvent was then removed and the crude product precipitated by addition of acetone. The crude was purified by repeated washing/centrifugation by water and acetone. Compound **4** was obtained as dark violet powder in 85% yield. M.p: > 300° C, ESI-MS *m/z* [M-1] = 647,8, ^{1}H NMR (D_2O + TEA) temp=70°C; δ ppm: 7.50 (bm 4H), 7.17 (bm 4H), 3.92 (bm 4H), 3.72 (bs 2H) 1.90 (bm, 12H). ESI-MS was performed on a Bruker 3000+ spectrometer. ^{1}H NMR was performed with a 400MHz Varian spectrometer.

Film preparation

The round glass coverslip substrates (Marienfeld laboratory glassware, Microscope cover glass) were cleaned by immersion in 100% ethanol overnight and then dried under argon flux. A 450 nm thick PMMA (Polymethyl methacrylate) film was spin-coated on the substrate in air and annealed for 12 h at 120 °C under controlled atmosphere. 40 μL of 1 mg/ml PDI-Lys water solution was drop-casted on PMMA and left to dry under laminar flux (ESP =254 m3 h^{-1}, LAF =0.4 m s^{-1}) overnight at RT (22–24 °C).

Two-contact device fabrication

Two-contact devices were fabricated in bottom-contact configuration (Scheme in Figure 2a). The substrates consisted of a 2.5 x 2.5 cm glass square and in Si/SiO_2 with 300 nm of oxide thickness. After cleaning the substrate by multiple sonications in acetone and 2-propanol, a 450 nm thick PMMA film was spin-coated on the glass substrate as described above. 70 nm thick gold and silver electrodes were deposited on top of the substrate under high vacuum at a base pressure of 10^{-6} mbar at a growth rate of 0.1 nm/s. 8 μl of PDI-Lys water solution 1 mg/ml was drop casted on top of gold electrodes and left to dry under laminar flux (ESP =254 m3 h^{-1}, LAF =0.4 m s^{-1}) overnight at RT (22–24 °C). Afterwards, the

film was washed with water and dried again to remove the TEA residue. Electrical characterization of the two electrode device was carried out using a SUSS probe station coupled to a B1500A Agilent semiconductor device parametric analyzer in an MBraun MB200gib N_2 filled glove box and in air. The conductivity of these devices was calculated as:

$$\sigma = \frac{L}{R \cdot W \cdot th} \tag{1}$$

where L = 70 μm was the channel length, R was the resistance, W = 1 cm was the channel width and th = 70 nm was the thickness of the electrode.[47]

PDI-Lys thin film characterization

To study the micromorphology Atomic Force Microscopy (AFM) measurements were performed with an NT-MDT NTEGRA Aura system in soft semi-contact (tapping) mode in ambient atmosphere conditions. The spring constant for the silicon tip was estimated with the Sader method[48] to be 2.9 N/m (NT-MDT NSG01). The scanning was performed at 50-60 nm oscillation amplitude setting (65% of the free amplitude at f_0). Sampling was set at 512x512 pixels. The absorption UV-vis spectra were recorded on a JASCO V-550 spectrophotometer. All the measurements were performed in air. For measuring spectra in N_2 environment, the substrate/film stack was first encapsulated in a glove box by using UV-curable epoxy resin. Then, the sample was taken out of the glove box and the spectra were measured in air. Spectra at different time points were obtained by removing the encapsulation and simultaneously monitoring the air exposure time. The peaks assignment was done by fitting each experimental UV-vis spectrum with multiple Lorentzian peak types. The thickness of the films, used for characterization experiments and cell culture was measured by performing profile measurements on three different samples (Profilmeter KLA Tencor) and its value was 244 ±38 nm. For the control film 50 nm thick P13 thin-films were sublimed under high vacuum in an Edwards 306 evaporator at a rate of 0.1 Å s and at a pressure of 5x 10^{-6} mbar on glass coverslip PMMA covered substrates. The optical images of the PDI-Lys film were taken with the Nikon Eclipse 2000-E microscope using a film fabricated as mentioned before.

Molecular mechanics and density functional theory (DFT) calculations

Molecular dynamics (MD) simulations on PDI-Lys molecules were based on a modified version of the all-atom OPLS force-field.[49–51] MD simulations were performed using the Berendsen thermostat and barostat with coupling time constants of 0.1 and 1.0 ps, respectively. Both the van der Waals and the Coulomb cut-off were set to 1.0 nm. The smooth particle-mesh Ewald approach[52] was used to compute long-range electrostatic interactions. The equations of motions were integrated according to the leap-frog algorithm, with a time step of 1 fs, as implemented in the Gromacs program package.[53] DFT and TD-DFT calculations were performed by applying the B3LYP[54,55] and M06-2X[56] approximations to the exchange-correlation functional and by using the 3-21G, 6-31G* and 6-31+G** basis sets for geometry optimizations, single-point energies and time-dependent calculations, respectively. Larger basis sets did not lead to significant improvement of computed transition energies.

Wettability Test

Contact angles of the cell culture medium (Dulbecco's Modified Eagle Medium (DMEM) supplemented with 10% v/v fetal bovine serum) on glass substrates coated with PDI-Lys film and PLL substrates were measured by using the static sessile drop method using a Digidrop GBX Model DS. For each film at least five drops

were measured. The cell culture medium droplets used for measurements had a volume of 1 μl.

Preparation of Rats Dorsal Root Ganglion Neuron Cultures

The experiments were performed according to the Italian law on protection of laboratory animals, with the approval of a local bioethical committee and under the supervision of a veterinary commission for animal care and comfort of the University of Bologna. Every effort was made to minimize the number of animals used and their suffering. Primary cultures of DRG neurons from postnatal p14-p18 rats (Sprague Dawley) were prepared by dissecting out DRGs as previously described [57], cleaning the individual ganglia of roots, and incubating them in type IV collagenase 5000 U/ml (Wentington) for 45-75 min at 37°C, 5% CO_2. DRGs were then dissociated gently with some passages through 0.5 mm and 0.6 mm sterile needles. After centrifugation, the DRG culture pellet was diluted in 1 ml of DMEM medium containing 10% Fetal Bovine Serum (FBS, Gibco). An equal amount of cell suspension was dropped onto 19 mm round glass coverslips and P13 pre-coated with 0,1 mg/ml poly-L-lysine (Sigma Aldrich), untreated P13 as controls and on pre-casted (see below) PDI-Lys placed in a 37°C, 5% CO_2 incubator. Cells were maintained in DMEM, (Gibco) supplemented with 10% FBS in the presence of 50 ng/ml NGF, and 1.5 μg/ml cytosine β-D-arabinofuranoside, (AraC, Sigma) to reduce glial cell expression.

Fluorescein-di-acetate (FDA) viability assay

DRG cell cultures plated on P13 and Per-Lys coated glass were incubated for 5 min with FDA (Sigma Aldrich). After rinsing with physiological saline, a sequence of images was taken after 3 and 5 days *in vitro* (DIV), using a Nikon Eclipse Ti inverted microscope equipped with a 20x objective and CoolSNAP EZ CCD camera. For cell counting analyses, thirty images were captured per condition, carried out in triplicates for each time point. Experiments were repeated three times. Results were analyzed using one-way analysis of variance (ANOVA).

DRG culture fixation and immunochemistry

DRG cultures plated on the different samples were fixed for 15 min with 4% paraformaldehyde (PFA) in 0.1 M phosphate buffered saline (PBS) at room temperature (RT, 20–24°C) and then rinsed with PBS. The samples were incubated for 20 min in 3% bovine serum albumin (BSA) and 0.1% Triton X-100 solution, before primary antibody incubation. The immunofluorescence stainings were done sequentially by using primary mouse-anti-GAP43 (1:100, Sigma-Aldrich) antibody, incubated over night at RT and secondary donkey anti-mouse Alexa Fluor 488-conjugated (1:1000, Molecular Probes-Invitrogen) antibody, incubated for 1h at RT. Coverslips were then mounted with Prolong Anti-Fade (Molecular Probes-Invitrogen). The optical images were taken with a Nikon TE 2000 inverted confocal microscope equipped with a 40x objective and 488 nm Ar^+ laser as excitation source.

Impedance measurements

The impedance measurements were performed at the OCP with the Fra32M module, incorporated in the Metrohm potentiostat/galvanostat Autolab PGSTAT128N, using Ag/AgCl and glassy carbon, respectively, as reference and counter electrode. The electrochemical cell was fabricated using Polydmethylsiloxane to standardize the tested area of the working electrode. The area of the working electrode exposed to 0,1M PBS solution was 20 mm^2 (2x10 mm). For the PDI-Lys electrode fabrication different solution concentrations (1, 0.5, 0.25, 0.125 mg/ml) were used applying the same procedure and substrates (glass, PMMA, Gold) as described above.

Cyclic voltammetry

0.5 mg/ml PDI-Lys films on gold electrode were analysed by three-electrode cyclic voltammetry measurements to determinate the electrochemical stability. An electrochemical workstation (Metrohm potentiostat/galvanostat Autolab PGSTAT128N) was used to apply a cyclic voltage from 0 to 600 mV with a scan rate set to 100 mV s^{-1}. The measurements were made with Ag/AgCl reference electrode and glassy carbon counter electrode.

Conclusion

In this work, we reported the synthesis, surface characterization and electrical properties of the PDI-Lysthin-film combined with its biocompatibility and its electrochemical behavior in physiological solution.. Remarkably, lysine functionalization of PDI promoted good filmability and electrical transport, crucial features for application as active layer in organic electronics. Indeed, casted films of PDI-Lys showed inert atmosphere electrical conductivities comparable to the ones measured for PDI-derivatives nanostructures with[21,25] or without[24] hydrazine treatment. Moreover, the ionic nature of the lysine framework enhanced the overall hydrophilicity of the final material, allowing a high *in vitro* biocompatibility and differentiation of the neural cells. When employed as electrode film coating PDI-Lys displayed smaller impedance and the same stability with respect to naked gold electrode at the electrode/electrolyte interface.

Electrochemical impedance properties on large area electrode, combined with biocompatibility and strong film stability in electrolyte solution, point out the potential of PDI-Lys for organic bioelectronics targeted to neural engineering applications.

Acknowledgements

Notes

*E-mail: simone.bonetti@bo.ismn.cnr.it

*E-mail: valentina.benfenati@isof.cnr.it

*E-mail: manuela.melucci@isof.cnr.it

References

1   G. Malliaras and R. Friend, *Phys. Today*, 2005, **58**, 53–58.
2   P. Ostoja, P. Maccagnani, M. Gazzano, M. Cavallini, J. C. Kengne, R. Kshirsagar, F. Biscarini, M. Melucci, M. Zambianchi and G. Barbarella, *Synth. Met.*, 2004, **146**, 243–250.
3   D. Khodagholy, T. Doublet, P. Quilichini, M. Gurfinkel, P. Leleux, A. Ghestem, E. Ismailova, T. Hervé, S. Sanaur, C. Bernard and G. G. Malliaras, *Nat. Commun.*, 2013, **4**, 1575.
4   V. Benfenati, S. Toffanin, S. Bonetti, G. Turatti, A. Pistone, M. Chiappalone, A. Sagnella, A. Stefani, G. Generali, G. Ruani, D. Saguatti, R. Zamboni and M. Muccini, *Nat. Mater.*, 2013, **12**, 672–80.
5   T. Cramer, B. Chelli, M. Murgia, M. Barbalinardo, E. Bystrenova, D. M. de Leeuw and F. Biscarini, *Phys. Chem. Chem. Phys.*, 2013, **15**, 3897–905.
6   L. Kergoat, B. Piro, M. Berggren, G. Horowitz and M.-C. Pham, *Anal. Bioanal. Chem.*, 2012, **402**, 1813–26.
7   S. Bonetti, A. Pistone, M. Brucale, S. Karges, L. Favaretto, M. Zambianchi, T. Posati, A. Sagnella, M. Caprini, S. Toffanin, R. Zamboni, N. Camaioni, M. Muccini, M. Melucci and V. Benfenati, *Adv. Healthc. Mater.*, 2015, **4**, 1190–1202.
8   C. D. Schmidt, C. Bòttcher and A. Hirsch, *European J. Org. Chem.*, 2009, 5337–5349
9   H. Langhals, *Helv. Chim. Acta*, 2005, **88**, 1309–1343.
10   P. a Lane, J. Rostalski, C. Giebeler, S. J. Martin, D. D. C. Bradley and D. Meissner, *Sol. Energy Mater.*, 2000, **63**, 3–13.
11   M. Barra, F. V. Di Girolamo, F. Chiarella, M. Salluzzo, Z. Chen, a. Facchetti, L. Anderson and a. Cassinese, *J. Phys. Chem. C*, 2010, **114**, 20387–20393.
12   X. Feng, Y. An, Z. Yao, C. Li and G. Shi, *ACS Appl. Mater. Interfaces*, 2012, **4**, 614–618.
13   C. Bonavolontà, C. Albonetti, M. Barra and M. Valentino, *J. Appl. Phys.*, 2011, **110**, 093715.
14   J. E. Anthony, A. Facchetti, M. Heeney, S. R. Marder and X. Zhan, *Adv. Mater.*, 2010, **22**, 3876–3892.
15   Z. Chen, Y. Zheng, H. Yan and A. Facchetti, *J. Am. Chem. Soc.*, 2009, **131**, 8–9.
16   R. Capelli, J. J. Amsden, G. Generali, S. Toffanin, V. Benfenati, M. Muccini, D. L. Kaplan, F. G. Omenetto and R. Zamboni, *Org. Electron. physics, Mater. Appl.*, 2011, **12**, 1146–1151.
17   S. Toffanin, V. Benfenati, A. Pistone, S. Bonetti, W. Koopman, T. Posati, A. Sagnella, M. Natali, R. Zamboni, G. Ruani and M. Muccini, *J. Mater. Chem. B*, 2013, **1**, 3850.
18   R. Li, W. Hu, Y. Liu and D. Zhu, *Acc. Chem. Res.*, 2010, **43**, 529–540.
19   Y. Guo, C. Du, C. Yu, C. A. Di, S. Jiang, H. Xi, J. Zheng, S. Yan, C. Yu, W. Hu and Y. Liu, *Adv. Funct. Mater.*, 2010, **20**, 1019–1024.
20   K. Sakakibara, J. P. Hill and K. Ariga, *Small*, 2011, **7**, 1288–1308.
21   Y. Che, A. Datar, X. Yang, T. Naddo, J. Zhao and L. Zang, *J. Am. Chem. Soc.*, 2007, **20**, 6354–6355.
22   A. L. Briseno, S. C. B. Mannsfeld, X. Lu, Y. Xiong, S. a. Jenekhe, Z. Bao and Y. Xia, *Nano Lett.*, 2007, **7**, 668–675.
23   C. Backes, F. Hauke and A. Hirsch, *Adv. Mater.*, 2011, **23**, 2588–2601.
24   Y. Sun, C. He, K. Sun, Y. Li, H. Dong, Z. Wang and Z. Li, *Langmuir*, 2011, **18**, 11364–11371.
25   M. Huang, U. Schilde, M. Kumke, M. Antonietti and H. Cölfen, *J. Am. Chem. Soc.*, 2010, **132**, 3700–7.
26   E. Bystrenova, M. Jelitai, I. Tonazzini, A. N. Lazar, M. Huth, P. Stoliar, C. Dionigi, M. G. Cacace, B. Nickel, E. Madarasz and F. Biscarini, *Adv. Funct. Mater.*, 2008, **18**, 1751–1756.
27   N. Gomez, J. Y. Lee, J. D. Nickels and C. E. Schmidt, *Adv. Funct. Mater.*, 2007, **17**, 1645–1653.
28   J. a. Schmidt and a. F. Von Recum, *Biomaterials*, 1991, **12**, 385–389.
29   M. Melucci, A. Sagnella, M. Zambianchi, M. Durso, T.

Posati, A. DelRio, A. Donnadio, A. Mazzanti, A. Pistone, G. Ruani, R. Zamboni and V. Benfenati, *RSC Adv.*, 2015, 63401–63406.

30   Y. Sun, Z. Li and Z. Wang, *J. Mater. Chem.*, 2012, **22**, 4312.

31   S. Chen, P. Slattum, C. Wang and L. Zang, *Chem. Rev.*, 2015, 151006144006000.

32   C. W. Struijk, A. B. Sieval, J. E. J. Dakhorst, M. Van Dijk, R. B. M. Koehorst, H. Donker, T. J. Schaafsma, S. J. Picken, A. M. Van De Craats, J. M. Warman, H. Zuilhof and E. J. R. Sudhlter, *Pulse*, 2000, **122**, 11057–11066.

33   M. Baldoni, A. Sgamellotti and F. Mercuri, *Org. Lett.*, 2007, **9**, 4267–4270.

34   T. H. Reilly, A. W. Hains, H. Y. Chen and B. a. Gregg, *Adv. Energy Mater.*, 2012, **2**, 455–460.

35   D. Schmidt, D. Bialas and F. Würthner, *Angew. Chemie Int. Ed.*, 2015, **54**, 3611–3614.

36   W. E. Ford, *J. Photochem.*, 1987, **37**, 189–204.

37   F. Pan, F. Gao, W. Liang and Y. Zhao, *J. Phys. Chem. B*, 2009, **113**, 14581–14587.

38   R. O. Marcon and S. Brochsztain, *Langmuir*, 2007, **23**, 11972–11976.

39   L. Zhong, F. Xing, W. Shi, L. Yan, L. Xie and S. Zhu, *ACS Appl. Mater. Interfaces*, 2013, **5**, 3401–3407.

40   M.-M. Shi, H.-Z. Chen, J.-Z. Sun, J. Ye and M. Wang, *Chem. Commun.*, 2003, **1**, 1710.

41   A. E. Clark, C. Qin and A. D. Q. Li, *J. Am. Chem. Soc.*, 2007, **129**, 7586–7595.

42   G. Melli and A. Höke, *Expert Opin. Drug Discov.*, 2009, **4**, 1035–1045.

43   C. E. Van der Zee, H. B. Nielander, J. P. Vos, S. Lopes da Silva, J. Verhaagen, a B. Oestreicher, L. H. Schrama, P. Schotman and W. H. Gispen, *J. Neurosci.*, 1989, **9**, 3505–3512.

44   M. M. R. Howlader, A. U. Alam, R. P. Sharma and M. J. Deen, *Phys. Chem. Chem. Phys.*, 2015, **17**, 10135–10145.

45   M. Sessolo, D. Khodagholy, J. Rivnay, F. Maddalena, M. Gleyzes, E. Steidl, B. Buisson and G. G. Malliaras, *Adv. Mater.*, 2013, **25**, 2135–9.

46   E. T. McAdams, J. Jossinet, R. Subramanian and R. G. E. McCauley, *Conf. Proc. Annu. Int. Conf. IEEE Eng. Med. Biol. Soc. IEEE Eng. Med. Biol. Soc. Annu. Conf.*, 2006, **1**, 4594–7.

47   C. Dionigi, T. Posati, V. Benfenati, A. Sagnella, A. Pistone, S. Bonetti, G. Ruani, F. Dinelli, G. Padeletti, R. Zamboni and M. Muccini, *J. Mater. Chem. B*, 2014, **2**, 1424.

48   J. E. Sader, J. W. M. Chon and P. Mulvaney, *Rev. Sci. Instrum.*, 1999, **70**, 3967–3969.

49   W. L. Jorgensen, W. L. Jorgensen, D. S. Maxwell, D. S. Maxwell, J. Tirado-Rives and J. Tirado-Rives, *J. Am. Chem. Soc.*, 1996, **118**, 11225–11236.

50   V. Marcon, D. W. Breiby, W. Pisula, J. Dahl, J. Kirkpatrick, S. Patwardhan, F. Grozema and D. Andrienko, *J. Am. Chem. Soc.*, 2009, **131**, 11426–11432.

51   A. Lorenzoni, M. Muccini and F. Mercuri, *RSC Adv.*, 2015, **5**, 11797–11805.

52   U. Essmann, L. Perera, M. L. Berkowitz, T. Darden, H. Lee and L. G. Pedersen, *J Chem Phys*, 1995, **103**, 8577–8593.

53   D. Van Der Spoel, E. Lindahl, B. Hess, G. Groenhof, A. E. Mark and H. J. C. Berendsen, *J. Comput. Chem.*, 2005, **26**, 1701–1718.

54   A. D. Becke, *J. Chem. Phys.*, 1993, **98**, 5648.

55   C. Lee, W. Yang and R. G. Parr, *Phys. Rev. B*, 1988, **37**, 785–789.

56   Y. Zhao and D. G. Truhlar, *Theor. Chem. Acc.*, 2008, **120**, 215–241.

57   V. Benfenati, S. Toffanin, R. Capelli, L. M. a Camassa, S. Ferroni, D. L. Kaplan, F. G. Omenetto, M. Muccini and R. Zamboni, *Biomaterials*, 2010, **31**, 7883–7891.

Journal of Materials Chemistry B Accepted Manuscript